

Near infrared imaging spectroscopy of NGC1275

Alfred Krabbe^{1,2}, Bruce J. Sams² III, Reinhard Genzel², Niranjan Thatte², and Francisco Prada³

¹ Deutsches Zentrum für Luft- und Raumfahrt, Institut für Weltraumsensorik und Planetenerkundung, Rutherfordstr. 2, 12489 Berlin-Adlershof, Germany

² Max-Planck-Institut für extraterrestrische Physik, Giessenbachstraße, 85748 Garching, Germany

³ Centro Astronomico Hispano-Aleman, Almeria, Spain

Received / Accepted

Abstract. We present H and K band imaging spectroscopy of the core regions of the cD/AGN galaxy NGC 1275. The spectra, including lines from H₂, H, ¹²CO bandheads, [Fe II], and [Fe III], are exploited to constrain the star formation and excitation mechanisms in the galaxy's nucleus. The near-infrared properties can largely be accounted for by ionized gas in the NLR, dense molecular gas, and hot dust concentrated near the active nucleus of NGC 1275. The strong and compact H₂ emission is mostly from circumnuclear gas excited by the AGN and not from the cooling flow. The extended emission of late-type stars is diluted in the center by the thermal emission of hot dust. The line ratios [Fe II]/Br γ , as well as [Fe II]/H₂ can be explained with X-ray excitation from the central AGN.

Key words: Galaxies: Individual NGC 1275 — Galaxies: Cooling Flows — Galaxies: Active — Infrared: Galaxies — Infrared: ISM: Lines and Bands — Instrumentation: Spectrographs

1. Introduction

NGC 1275 (Perseus A, 3C 84) at the center of the Perseus cluster has been variously classified as an active galaxy, a merger, a cooling flow galaxy, a BL Lac object, and an FRI radio jet source. However, many of its physical characteristics — from X-ray to radio — remain baffling. NGC 1275 exhibits the characteristics of several source types: Seyfert (1943) included it in his original list, Minkowski (1957) called it a galaxy “collision”. The dominant low velocity (LV) component ($\approx 5200 \text{ km s}^{-1}$) is the giant cD elliptical NGC 1275, the other component (HV, $\approx 8300 \text{ km s}^{-1}$) is probably a nearby spiral galaxy (at least partially) in front of the main galaxy (Haschick et al. 1982). Veron (1978) suggested that NGC 1275 was a BL Lac object, while other authors have suggested that it was more compatible with LINERs (e.g. Norgaard-Nielsen et al. 1990).

Send offprint requests to: A. Krabbe; krabbe@dlr.de

NGC 1275 has a powerful, nearly point like X-ray emitting nucleus with a flux of $L_X \approx 2 \times 10^{43} \text{ erg s}^{-1}$ (Prieto 1996), which is embedded in an extended halo of diffuse X-ray emitting intracluster gas. The nucleus of NGC 1275 is displaced by about 25'' from the center of symmetry of the large scale ($\sim 2'$) cluster gas halo, perhaps due to its peculiar motion through the gas (Böhringer et al. 1993). Temperature profiles of the X-ray halo suggest that a “cooling flow” of $\approx 200 \text{ M}_\odot \text{ yr}^{-1}$ is condensing out of the surrounding intracluster medium onto the galaxy (Fabian et al. 1981, Cardiel et al. 1995). As in all cooling flow galaxies, the ultimate fate of this purported inflowing material is unclear, but visible band colors and Balmer absorption lines spectra characteristic of A0 stars show that at most 10% of the gas can form stars with a standard Salpeter IMF (Romanishin 1986). NGC 1275 is unique among cooling flow galaxies in that it in fact shows evidence of ongoing star formation.

Even by the standards of infrared luminous mergers, NGC 1275 has very powerful, extended H₂ emission (Fischer et al. 1987) matched only by NGC 6240 (van der Werf et al. 1993). In NGC 1275, this emission has been speculated to have its origin in the cooling flow, although fast J-shocks, UV pumping, and X-ray heating via supernovae and/or AGN also produce strong H₂ emission. Merging events are a likely mechanism for supplying NGC 1275 with substantial ($M \gtrsim 3 \times 10^9 \text{ M}_\odot$) quantities of H₂ in giant molecular clouds which are detected through mm wave CO observations within the central regions (Inoue et al. 1996). CO data also show two kinds of motion: a large ($\gtrsim 5 \text{ kpc}$) scale rotation which has been attributed to merging/cannibalism, and smaller scale turbulence, attributed to the inflow of cooling flow gas (Reuter et al. 1993). Recent 2.6 mm CO interferometric observations reveal the majority of the gas to be in a ring structure of radius $\approx 4''$ oriented in the East-West direction. The ring has a westerly extension up to 30'' from the nucleus, and nearly 80% of the total CO is on the western side (Inoue et al. 1996). Very deep interferometric observations of the nucleus itself show no CO absorption from very cold gas, which puts very tight limits on any mass deposition from

Table 1. Observations of NGC 1275 with the MPE 3D imaging spectrograph.

Date	Band	t_{int} sec	Seeing	Spectral/Flux Calibrator	mv
15/01/95	K	2400	1''.4	Mel 20497 (F6V)	6.9
15/01/95	H	1100	1''.5	Mel 20497 (F6V)	6.9
16/01/95	K	2000	1''.5	PPM 45428 (F8V)	4.1
16/01/95	H	1200	1''.6	Mel 20497 (F6V)	6.9
21/01/95	H	2400	1''.1	Mel 20497 (F6V)	6.9

a cooling flow if the gas cools to nearly 3 K (Braine et al. 1995).

NGC 1275 is a Fanaroff-Riley type I (F–RI) radio source with powerful (≈ 0.4 Jy at 22 cm) radio lobes ≈ 10 kpc long and oriented at position angle (PA) 160° which emanate from a central core (Pedlar et al. 1990). The asymmetry of the radio lobes and their spectral indices suggest that we are looking nearly pole-on at the central F–RI radio engine (Pedlar et al. 1990, Levinson et al. 1995). Within the central $30''$ region, relativistic particles and the magnetic field from the bipolar radio lobes produce a pressure, which exceeds the thermal gas pressure and so must disturb any cooling flow within that region (Pedlar et al. 1990, Böhringer et al. 1993). At even smaller scales, VLBI imaging shows that the central core ($\approx 1''$) breaks up into many smaller components and a southern/northern jet pair (Venturi et al. 1993, Vermeulen et al. 1994). Recently, a new component has been discovered only 55 mas south of the central peak (Taylor & Vermeulen 1996). Near infrared (NIR) annular photometry shows that the nuclear K-band light is dominated by non stellar emission which could be either thermal emission from hot dust, or optically thin synchrotron radiation (Longmore et al. 1984). Recent *HST* observations in the UV show that any nuclear engine/star cluster must be < 17 pc in size (Maoz et al. 1995).

Our goal in this work is to better constrain the many existing models of NGC 1275 with near infrared (NIR) imaging spectroscopy and spectral synthesis modeling. In dusty environments, NIR imaging has optical depth penetration 10 times deeper than visible wavelengths, and NIR spectroscopy is sensitive to a wealth of diagnostic lines which describe the physical state of the gas and stars in the nucleus. Throughout this paper we assume a scale of $344 \text{ pc}''^{-1}$ ($H_0 = 75 \text{ km s}^{-1} \text{ Mpc}^{-1}$, $z = 0.0172$).

2. Observations and data reduction

We observed NGC1275 using the Max-Planck-Institut für extraterrestrische Physik (MPE) imaging spectrometer 3D and the Max-Planck-Institut für Astronomie (MPIA) tip-tilt image tracker “CHARM” on 1995 January 15, 16 and 21 at the 3.5m telescope of the Max-Planck-Institut

für Astronomie at Calar Alto, Spain. The CHARM instrument (McCaughrean et al. 1994) removes atmospherically induced image motion and produces stable images of increased spatial resolution. We locked CHARM on the bright point-like nucleus of NGC1275, and corrected at 5 Hz. Under seeing conditions varying from 1.0 to $1''.7$, we achieve a final overall image quality of FWHM $1''.5$ as determined by fitting to the point-like nucleus (Maoz et al. 1995). The “3D” instrument (Krabbe et al. 1995, Weitzel et al. 1996) is an field imaging spectrograph which provides, during in a single exposure, H or K band data cubes with spectral resolution of $R = \lambda/\Delta\lambda = 1000$ and 2000. The two spatial cube dimensions are 16 pixels on a side, with pixel sizes selected to be $0.5''$ (giving an $8'' \times 8''$ field of view), while the third dimension of 256 pixels is spectral. The intrinsic spectral sampling of the camera is with pixels of size λ/R , so by dithering the spectral sampling by 1/2 pixel on alternate data sets, we achieve fully Nyquist sampled spectra. The spectral resolution, achieved with the current reduction procedure, is 670, or 450 km s^{-1} ; future software will produce full $R = 1000$ spectra after co-addition. For extended objects, the efficiency gain over a long slit spectrograph is substantial, as at any point within our $8'' \times 8''$ field, it is possible to obtain the full band object spectrum.

The data (Table 1) frames were interleaved with identical sky exposures $60''$ away to the West. The source observations were preceded and/or followed immediately by a set of spectral calibration observations of nearly featureless stars of known brightness. The few known spectral features in the reference star spectra (e.g. $\text{Br}\gamma$ in K band and $\text{Br}9 - \text{Br}11$ in H band) were later removed by interpolation. A temporally variable deep CO_2 absorption near $2.01 \mu\text{m}$ made accurate sky subtraction in this regime difficult. In addition, the temporal variability of OH lines in the H band produces spurious sky noise which dominates the background across the band.

A run-down on typical 3D data reduction with the Groningen GIPSY software is given in Weitzel et al. (1996). Spectral baselines were calibrated using the color temperature of the calibrator stars and a featureless Nernst glower. The absolute wavelength calibration is accurate to better than 1/4 pixel. Individual data sets were properly weighted, registered onto the central peak of NGC 1275, and co-added.

The K and H band spectra of the nucleus within a $3''$ aperture are presented in Figs. 1 and 2, which present the enormous variety of emission and absorption lines. The signal to noise in the K-band spectrum is ≈ 70 in the continuum. For the H band, the signal to noise is ≈ 25 in the continuum.

3. Nature of the continuum emission

Fig. 3 represents the true, line emission free, K band continuum structure of NGC 1275. Its peaking at the nucleus

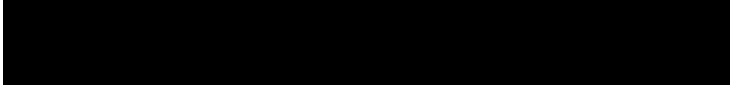


Fig. 1. K band spectrum of the central 3'' of NGC 1275. This aperture contains nearly all of the line flux. A linear baseline continuum of mean value 9.0×10^{-16} erg s $^{-1}$ cm $^{-2}$ Å $^{-1}$ has been removed.



Fig. 2. H band spectrum of the central 3'' of NGC 1275. This aperture contains nearly all of the line flux. A linear baseline continuum of mean value 1.3×10^{-15} erg s $^{-1}$ cm $^{-2}$ Å $^{-1}$ has been removed.

confirms that the bulk of the emission arises in the central 300 pc. The slight south-east north-west extension, almost along the radio PA of 160° (Pedlar et al. 1990), is 2σ significant.

We analyzed the the continuum spectrum with respect to contribution from stars, the active galactic nucleus, hot dust from the circumnuclear environment, and free-free emission. K and M stars ($T_{\text{eff}} \approx 4000$), dominating the K band stellar emission, show strong CO absorption features in their more or less BB spectrum which can be used to constrain the fraction of total light originating in stars. NIR spectra from AGN show a power law spectrum of the form $I_{\lambda} \propto \lambda^{\alpha}$ where α varies between -0.5 and -1.5 (Laor & Draine 1993, Acosta-Pulido et al. 1990). Hot dust in this context is mainly referred to as being reprocessed radiation from AGN and, to a minor extent, from starburst activity. It's spectrum is that of a black body multiplied

by a power-law emissivity of the form $\epsilon_{\text{dust}} \propto \lambda^{-1}$. From these contributions a synthetic galaxy spectrum including extinction effects has been modelled and (least square) fitted to the observed continuum spectrum. Details of the procedure are given in the appendix, contrains on the parameters are being discussed below, and the results are presented in Sect. 3.2.

3.1. Physical constrains on the continuum emission

The size of the search space was reduced by placing constrains on the total extinction, Galactic extinction, free-free contribution, dust temperature, and stellar populations.

i) The Galactic extinction toward NGC 1275 is $A_B = 0.7$, or $A_V = 0.53$, and there is an additional component of extinction intrinsic to NGC 1275 itself. From

Table 2. Line strengths in the central 3'' aperture

Species	λ^a	Width ^b	F ^c	σ_F
FeII 1.534	1.5335	660	1.3	0.5
FeII 1.644	1.6439	526 ^d	63	2.5
H ₂ 1–0 S(7)	1.7480	256	11	0.7
Br δ	1.9446	263	3.1	0.5
H ₂ 1–0 S(3)	1.9576	301	42.5	2.5
H ₂ 1–0 S(2)	2.0338	225	14.4	0.7
HeI	2.0584	519	2.8	0.5
H ₂ 2–1 S(3)	2.0735	183	3.1	0.6
H ₂ 1–0 S(1)	2.1219	238	41.1	2.5
H ₂ 2–1 S(2)	2.1540	517	3.4	0.5
Br γ	2.1661	982	9.7	2.5
H ₂ 3–2 S(3)	2.008	207	1.3	0.5
H ₂ 1–0 S(0)	2.2231	328	10.0	0.7
FeIII 2.244	2.243	504	2.2	0.5
H ₂ 2–1 S(1)	2.2473	754	7.7	0.6

^a μm observed corrected for $z = 0.0172$ ^b km s^{-1} corrected for instrument resolution of 450 km s^{-1} .Width error typically $30 - 50 \text{ km s}^{-1}$ ^c $10^{-15} \text{ erg s}^{-1} \text{ cm}^{-2}$ ^d Best fit of single Gaussian. Two component fit of $1345 \pm 120 \text{ km s}^{-1}$ and $280 \pm 22 \text{ km s}^{-1}$ is superior. See text.

UV measurements we have $E(B-V) = 0.2 - 0.3$ (Maoz et al. 1995, Levinson et al. 1995), which both suggest that $A_V \approx 1.0$ at the nucleus. Integrated over the central stellar area, H-K is 0.15 redder than typical ellipticals (Longmore et al. 1984), which requires $A_V \approx 2.4$. Hence we constrain the V band extinction to $A_V < 2.0$, or $A_K < 0.2$ (Rieke & Lebofsky 1985). Since we know that the central light is likely to be dominated by the AGN (Longmore et al. 1984), we choose to use a screen model of extinction there, while farther out at distances $\gtrsim 500 \text{ pc}$ we will use a mixed stars/gas model.

ii) The free-free continuum can be obtained from the Br γ line flux using case B recombination and assuming $T = 10000 \text{ K}$. (Joy & Lester 1988) have shown that this method gives consistent results compared to a NIR multi-color continuum decomposition (Joy & Harvey 1987) and radio measurements (Wynn-Williams & Becklin 1986). Using the Br γ line flux from Table 2 we can thus constrain the free-free contribution to be about 2% of the underlying continuum. There is some suggestion that the free-free emission could be higher in NGC 1275 because the central plasma is constantly being replenished with free electrons via the cooling flow gas. However, if there were a substantial population of such ions, they would contribute to the scattering of the central source at the 1% level (Sarazin & Wise 1993), which would in turn produce a blue excess. If the 1% scattering is responsible for the observed nuclear blue excess of $\sim 10^{44} \text{ erg s}^{-1}$ (Crawford & Fabian 1993), then the central source would require an X-ray/UV luminosity of roughly $10^{46} \text{ erg s}^{-1}$, which is ≈ 600 times the

**Fig. 3.** The K band continuum of NGC 1275. Orientation: N up, E left. FWHM 1''.6. Field of view 8'' \times 8''. Contours are at 1.25, 2.5, 5, 10, 20, 30...% of peak flux of $8.5 \times 10^{-15} \text{ erg s}^{-1} \text{ cm}^{-2} \text{ arcsec}^{-2}$.

point X-ray luminosity. Hence we set the free-free emission to a typical value of $< 3\%$ of the total continuum, or sometimes ignore it completely, as our fits constrain the relative contributions to only $\approx \pm 10\%$. Had we not done so, the free-free and AGN emission would have traded off influence with each other, as they are both power laws of similar slopes.

iii) Hot dust has turned out to be very common in the nuclear regions of AGNs (Granato et al. 1997, Maiolino et al. 1995) and, to some extent, in starburst galaxies as well (see e.g. Böker et al. 1998). It surrounds the nucleus forming a torus which absorbs radiation from the AGN and reemits it in the mid-infrared. Since hot dust too close to the AGN will start to sublime, the maximum dust temperature is set by the sublimation temperature of the dust material. Silicate and graphite grains, which are the main constituents of interstellar dust (Laor & Draine 1993), will sublime at temperatures of about 1400K and 1750K resp., setting the limit for the the dust temperature at about 1500K at the inner edge of the dust torus. The minimum radius for dust grains to survive is $\gtrsim 0.2L_{46}^{1/2} \text{ pc}$ (Laor & Draine 1993), where L_{46} is the central source bolometric luminosity in units of $10^{46} \text{ erg s}^{-1}$. For NGC 1275 with $L_{46} = 0.04$ (Levinson et al. 1995), this is $\gtrsim 0.05 \text{ pc}$. The dust temperature observed will be a mixture of dust at different temperatures along the line of sight weighted with their column density distribution. Thus the effective temperature will be lower and, e.g. for NGC 1068, in the

range of 700 K (Thatte et al. 1997). As NGC1275 is a F–R I type radio source, we are probably looking nearly pole on at the central source, and hence see the largest possible fraction of the hot inner surfaces of the clouds which make up an obscuring torus (Pier & Krolik 1992), suggesting that we limit the temperature of the dust in our simulations to a relatively high value of 1000 K.

iv) The NIR flux of essentially all integrated galaxy populations is dominated by giants and, to a lesser extent, by supergiants (Oliva et al. 1995). We rule out K5 V stars because for all reasonable stellar populations they are too faint to contribute substantially to the overall H and K band fluxes. As an underlying stellar population we choose K5 III stars because they dominate, to first order, the light of nearly all galaxies at H and K bands (Frogel et al. 1978, Oliva et al. 1995). This is due to the fact that their effective temperatures of ≈ 4000 K have a black body emission peak in those bands, and because they are typically 200 times brighter than K5 V stars with similar effective temperatures. Digitized libraries of NIR stellar spectra are available in the K band 1986, so we used the spectrum of the K5 III star γ Dra as our template I_λ^{STAR} in the K band.

In the H band, no such digitized stellar library was publicly available at the time of this data reduction, so we constructed a continuum spectrum appropriate to the stellar population of NGC 1275 by summing the contributions of many black body curves of different temperature scaled by the fractional number of stars having that temperature. This produces a continuum spectrum without any lines. The H band CO absorption features are relatively weak, so they would have contributed little to the fitting anyway. The galaxy population, necessary for this procedure, was modeled with the stellar population evolution code STARS (Sternberg & Kovo, in preparation). Given a set of input parameters it determines the binned number density function of stars in the HR-diagram. Summing the series of appropriately scaled black body curves at the various temperatures results in a H-band continuum that approximates the underlying H band continuum of NGC 1275, if the input parameters to STARS are varied adequately. The composite spectrum is then normalized to the same wavelength as the K band stellar library spectrum in order to produce the final H and K band underlying stellar spectrum, I_λ^{STAR} . All K spectra are normalized to a wavelength of $2.27 \mu\text{m}$, and all H spectra are normalized to $1.57 \mu\text{m}$, which we chose because the spectra are free of lines there.

3.2. Decomposing the continuum emission

In the central $1''$ (0.3 kpc) region we expect that the contribution of the AGN overwhelms the the stellar population. This is indeed the case, as the continuum emission from the center of NGC 1275 is well modeled by the light of



Fig. 4. Spectral fitting to the NGC 1275 spectrum in an aperture of $1''$ centered on the nucleus. Best fit is achieved with a relative stellar contribution of 0.0, an AGN power-law (see text) contribution of 0.5, a hot dust contribution of 0.5 at 700 K, and a K-band extinction of 0.05 (screen model). The plot shows (in decreasing order from the top) a) the raw spectral data; b) the final derived model fit to the continuum; c) the statistical weights given to each data point; d) the derived power-law component of the model; e) the derived dust component of the model; f) the residuals between model and data. Note that because we are fitting the continuum, not the lines, the weights in regions of strong line emission have been set to zero (cf Eq. (A4)). The spectra are all normalized at $\lambda = 2.27 \mu\text{m}$, so the relative contributions of the various components can be read off at that wavelength.

K5 III or K5 Ib stars heavily diluted by emission from hot dust and AGN typical power-law emission (Fig. 4). The best fitting values are $c^{\text{STAR}} = 0.0 \pm 0.1$, $c^{\text{PL}} = 0.5 \pm 0.1$, $c^{\text{HD}} = 0.5 \pm 0.1$, $T_d = 700 \pm 200$, $\tau_K = 0.05 \pm 0.1$, where the c_i represent fractional contributions and were the errors are those derived from the estimated systematic errors in the spectra and from multiple trials with slightly varied weights and initial guess parameters. The relative insignificance of spectral features in the underlying stellar population shows that the fitting process at the nucleus is dominated by the power laws, and that we are unable to distinguish between the various possibilities of underlying populations. The relative contribution of power-law emission is not particularly sensitive to the adopted AGN spectral index (-0.5 through -1.5, see appendix), because its main function is to dilute the very steep slope of the stellar continuum (very nearly a black body).

In contrast, the same fitting process applied to a $1''$ wide annulus $3''$ (0.9 kpc) from the nucleus yields completely different result. Because the CO absorption band-heads are clearly observed in the K band spectrum (they are much less diluted), we fit this region only using the K band data. The fit is excellent (Fig. 5), and yields the fol-



Fig. 5. Spectral fitting to the NGC 1275 spectrum in a 1'' wide annulus of radius 3'' centered on the nucleus. Best fit is achieved with a relative stellar contribution of 0.6, an AGN power-law (see text) contribution of 0.4, a hot dust contribution of 0.0, and a K-band extinction of 0.01 (mixed stars and gas model).

lowing contributions: $c_{\text{STAR}} = 0.6 \pm 0.1$, $c_{\text{PL}} = 0.4 \pm 0.1$, $c_{\text{HD}} = 0.0 \pm 0.1$, $\tau_{\text{K}} = 0.01 \pm 0.1$, where we have chosen to apply a mixed stars/gas model of extinction rather than a simple screen. Again, we assume a K5 III star dominated underlying stellar population. Note that the AGN contribution could also be interpreted as free-free emission at this distance from the nucleus, where we do not expect any direct or scattered contribution from the AGN. By the time we reach 4'' (1.2 kpc) from the nucleus, the stellar component dominates completely, and we find $c_{\text{STAR}} = 0.90 \pm 0.1$, $c_{\text{PL}} = 0.1 \pm 0.1$, $c_{\text{HD}} = 0.0 \pm 0.1$, $\tau_{\text{K}} = 0.01 \pm 0.1$. Hence the behavior of the the various components is as expected from a central AGN dominated source.

4. The H_2 emission

The H_2 emission in NGC 1275 is exceptionally luminous (Fischer et al. 1987) even if compared with other powerful H_2 emitting galaxies. The excitation of H_2 in AGNs is usually explained to be a mixture of shocks (Brand et al. 1989), UV photons (Sternberg & Dalgarno 1989), and X-rays (Draine & Woods 1991). The shocks can be caused by galaxy merging or by supernovae, the UV radiation could come from OB star associations (Puxley et al. 1990), while only an AGN with a black hole can produce the quantities of X-ray radiation needed to excite the H_2 seen in Seyfert nuclei.

4.1. Spatial distribution of H_2 emission

The H_2 line emission (Fig. 6) is strongly dominated by an unresolved source centered on the nucleus surrounded by weak extended emission extending a few arcseconds

Fig. 6. Line map of the H_2 1–0 S(1) transition. The emission is almost completely symmetric, with FWHM of 1''.6. The other H_2 transitions show similar structure and extent. Contours are at 2.5, 5, 10, 20, 30...% of peak flux of 2.1×10^{-14} erg s $^{-1}$ cm $^{-2}$ arcsec $^{-2}$.

west. The fact that the primary exciting source is not distributed over scales $\gtrsim 300$ pc suggests that most of the H_2 emission is associated with the circumnuclear environment and probably the active galactic nucleus and not, as speculated before (Inoue et al. 1996) with the cooling flow. The low level extended emission reach $\approx 2\%$ of the peak flux at our limiting distance of 5'' or 3.5 kpc (Fig. 7). The total H and K band H_2 emission amounts to 1.3×10^{-13} erg s $^{-1}$ cm $^{-2}$ (see Table 2) or, for a distance of 70 Mpc, a total luminosity of $\text{L}_{\text{H}_2} = 8 \times 10^{40}$ erg s $^{-1}$.

4.2. Excitation of the H_2 emission

The high signal-to-noise in our spectra allow us to check the effective excitation temperature from the column density of molecules in each quantum state (see e.g. Beckwith et al. 1978):

$$N_{\text{col}} = 4\pi I / A_{\text{ul}} h\nu \quad (1)$$

where I is the surface brightness in the line and A_{ul} is the Einstein A coefficient. The surface brightnesses have been dereddened using $A_V = 2.0$ (Sect. 3.1) as a realistic value. Screen and mixed extinction models (McLeod et al. 1993) for the dereddening gave flux correction between 10% and 20%. Since the appropriate model was uncertain, the correction was averaged between screen and mixed model and the uncertainties propagated in the errors.

Table 3. Column density and temperature analysis of H₂

Line	A _{ul} ^a	N _{col} ^b	ln(N _{col} /gu)	T _{Tex} ^A
1-0 S(0)	2.5(-7)	3.8(15)	43.47	6472
1-0 S(1)	3.5(-7)	1.1(16)	43.09	6951
1-0 S(2)	4.0(-7)	3.2(15)	42.72	7585
1-0 S(3)	4.2(-7)	8.7(15)	42.42	8365
1-0 S(7)	3.0(-7)	2.9(15)	40.79	12817
2-1 S(1)	5.0(-7)	1.5(15)	41.10	12551
2-1 S(2)	5.6(-7)	5.6(14)	40.98	13150
2-1 S(3)	5.8(-7)	4.9(14)	39.53	13887
3-2 S(3)	5.6(-7)	2.0(14)	38.66	19089

^a Turner et al. 1977^b cm⁻²; H₂ flux dereddened with A_V = 2.0

Fig. 7. Azimuthally averaged profile of the H₂ 1-0 S(1) emission. There is a very low level extended component to the emission, which reaches a few percent of the peak flux at $r = 4''$.

In thermal equilibrium, the line ratios should be given solely by the number of atoms in each quantum state and their spontaneous emission coefficients if the H₂ is optically thin. From Table 4.2 we conclude that this is indeed the case. The column densities are always lower than $N_{\text{col}}(\text{H}_2 \text{ 1-0 S(1)}) = 9.6 \times 10^{15} \text{ cm}^{-2}$. Summing over all the observed H₂ lines gives $N_{\text{col}}(\text{H}_2^{\text{hot}}) \approx 3 \times 10^{16} \text{ cm}^{-2}$. If we assume that this gas is uniformly distributed within the emitting region, then the total mass of contributing H₂ would be $\sim 1000 \text{ M}_{\odot}$.

In Fig. 8 we plot the natural log of N_{col} per mode against the energy of the upper level given as a temperature (compare with Kawara & Taniguchi 1993). The error bars include the errors given in Table 1 and the dereddening. The inverse slope is the effective excitation temperature Tex of the gas and corresponds to the kinetic temperature if local thermal equilibrium (LTE) prevails.

Depending on the conditions within a molecular cloud, the initial ortho/para ratio of 3 of molecular hydrogen at formation may evolve and eventually drop to lower values (Martini et al. 1997). Exchange reactions with H and H⁺ (Flower & Watts 1984) or a low temperature environment ($T \lesssim 200 \text{ K}$; Burton et al. 1992) can even lower the ratio to below 2.0 (see e.g. Hora & Latter 1996). A high temperature environment in turn will keep the ortho/para ratio at 3. In a photodissociation region (PDR), however, freshly exposed H₂ may keep the ortho/para ratio down (Chrysostomou et al. 1993) although the environment is hot. In Fig. 8 the column densities have been divided by

the statistical weights corresponding to their states which include the spin degeneracies $g_s = 1$ for even (para) and $g_s = 3$ for odd (ortho) J. If the ortho/para ratio in the molecular hydrogen is 3:1 then the ortho and para column densities should lie along a line. For the 1-0 transitions, where we have enough data points, this is indeed the case. This demonstrates that the either the molecular hydrogen has just been formed or that the H₂ has been kept in a high temperature environment.

The distribution of data in Fig. 8 shows that the H₂ gas is nearly isothermal. Below 8000 K upper level energy, the excitation temperature is Tex $\approx 1500 \text{ K}$, but above 8000 K, Tex does only vary between $\approx 2600 \text{ K}$ and $\approx 2900 \text{ K}$. If no extinction correction is applied, the temperatures come out to be 1450 K, 2400 K, and 2650 K resp., which is still in agreement with the 1σ errors given in Fig. 8. All data (except for 2-1 S(3), see below) out to level energies of $\approx 20000 \text{ K}$ lie along an only slightly curved line. In particular, the column density per mode of 1-0 S(7) is close to those of 2-1 S(1) and 2-1 S(2), indicating that the rotational and vibrational temperatures are about the same and the fluorescent excitation of the gas is rather small (Draine & Bertoldi 1996). The proposed likely mechanism to populate the levels of this hot H₂ gas with Tex $\leq 2700 \text{ K}$ is collisional excitation in a post shock environment, which has been observed in many galactic sources (see e.g. Fischer et al. 1987, Gredel et al. 1994, Wright et al. 1996). However, at column densities prevailing in the central 300 pc of NGC 1275, a PDR scenario cannot be completely excluded. In dense PDRs, the vibrational ladder is thermalized while the rotational ladder in a given vibrational state may be out of thermal equilibrium (see e.g. Timmermann et al. 1996). The fact that we do not see gas of temperature above 5000 K (Wright et al. 1996) may, however, indicate that the contribution of nonthermal processes (UV pumping) to the H₂ excitation is rather moderate.

The excitation conditions in NGC 1275 can be investigated in more detail by examining the ratio of two ortho or para lines and put them in context. The remaining uncertainty introduced by the intrinsic ortho-para ratio of the gas clouds can thus be avoided (Mouri 1994). Locating these ratios in a ortho-para line ratio plane provides an independent guide for distinguishing between the relative contribution of X-ray heating, shocks, and UV pumping excitation of H_2 gas in starburst and AGN galaxies (Fig. 9). As non thermal processes (e.g. UV pumping in low density gas) excite high vibrational states more easily than the thermal process, the ratio of two ortho transitions such as $R_O = H_2 2-1 S(1)/H_2 1-0 S(1)$ gives an ortho-para balance independent measure of the relative contribution of thermal and non-thermal processes. The same holds for $R_P = H_2 1-0 S(2)/H_2 1-0 S(0)$. The expected value of R_O in the case of pure non thermal excitation under nearly all realistic conditions is $R_O = 0.56$ (Black & van Dishoeck 1987), while thermal UV excitation gives a value of R_O near 0 (Sternberg et al. 1987). From Table 2, we find $R_O = 7.7/41.1 = 0.19$ and $R_P = 14.4/10.0 = 1.4$, which again, as we noted earlier, puts NGC 1275 in the $R_O - R_P$ plane close to the location of NGC 6240 (Fig. 9). Starburst galaxies like NGC 253 and galactic photodissociation regions generally show $R_P \leq 1.0$. Following this method one can also define a ratio, $R_O = H_2 1-0 S(3)/H_2 1-0 S(1)$, of two ortho lines which is again independent of the initial ortho-para ratio in the molecular clouds. When placed in this diagram (Fig. 9), NGC 1275 falls near other powerful AGNs like NGC 1068.

The interpretation of these diagrams tells us that the excitation is mostly “thermal”, with a small component appearing as “nonthermal emission”. The gas must then be quite dense, with $n_T \gtrsim 10^5 \text{ cm}^{-3}$. The placement of NGC 1275 near other powerful AGN and merger galaxies suggests that both X-ray and shock mechanisms may be at work creating the powerful H_2 emission. Hence, based on the spatial extent of the H_2 emission and its temperature, we propose that there are two distinct sources of H_2 excitation: the AGN nucleus, which excites the vast majority of the radiation, and which produces the compact emission core seen in our maps, and the extended region of moderate star formation which excites the highly extended, weak H_2 envelope.

4.3. $H_2 2-1 S(3)$ line strength

The column density of the $H_2 2-1 S(3)$ line is lower by a factor of 3 compared to what could be expected from weighted extrapolation of the $2-1 S(1)$ and $2-1 S(2)$ transitions. Even if the ortho/para ratio within the $2-1$ transitions is not close to 3, which it was in the $1-0$ transitions, $N_{\text{col}}(2-1 S(3))$ is still a factor of > 2.5 lower compared to $N_{\text{col}}(2-1 S(1))$ and using $\text{Tex} = 2600 \text{ K}$ for the two ortho states. Inspecting the original data and the spectrum in Fig. 1 did not show any abnormalities. Since the chance

for blending the line with a strong absorption can be excluded for this part of the spectrum and the atmosphere, we argue that this weakness of the $H_2 2-1 S(3)$ line is real. Inspecting Fig. 5 reveals that the $2-1 S(1)$ line is also weak outside the nucleus at a radius of $\approx 1 \text{ kpc}$. It would be visible if it was 2.5 time stronger or about half the strength of the $1-0 S(2)$ line, which is clearly present.

The only other galaxy, were a weak $H_2 2-1 S(3)$ line has been reported so far, is NGC 6240 (Lester et al. 1988), although only as an upper limit. From their Table 3 one can estimate that the column density of $2-1 S(3)$ line in NGC 6240 is at least 3.5 times weaker than expected from extrapolating other data, which is in good agreement with our finding and suggest that there may be a common mechanism at work. The column densities in NGC 6240 are only a factor of 2 higher compared with NGC 1275 and their derived temperature range is almost identical with Fig. 8. It should be noted, however, that the excitation conditions in both galaxies are not identical. Draine & Woods (1990) have shown that in addition to X-ray heating, UV pumping plays a major role in NGC 6240. This is already indicated in Fig. 9 as well as and in Fig. 4 of Lester et al. (1988): The large offset between the line through the $1-0$ transitions and the $2-1$ data is different from NGC 1275 (Fig. 8). Recently, Sugai et al. (1997) reported that they were unable to confirm the weakness of the $H_2 2-1 S(3)$ line in NGC 6240 with $R = 580$ grism spectroscopy. Better quality data at higher spectral resolution is certainly required to clarify the situation.

The most likely mechanism for the weakness of the $H_2 2-1 S(3)$ line is resonant fluorescent excitation of the upper level ($\nu = 2, J = 5$) by $\text{Ly}\alpha$ photons (Black & van Dishoeck 1987). The $\text{Ly}\alpha$ photons needed for this pumping process can easily be provided in an environment where a notable fraction of the H_2 is excited by X-ray heating (Black & van Dishoeck 1987). Although detailed models of resonant fluorescent excitation of the $\nu = 2, J = 5$ level does not exist, the weakness of the $H_2 2-1 S(3)$ line by itself already demonstrates that at least in the nuclear region the excitation of the molecular hydrogen in NGC 1275 is dominated by the central AGN. This is in agreement with our previous finding that the excitation environment in the nuclear region of NGC 1275 is much more dominated by X-ray heating than in NGC 6240 (Draine & Woods 1990). NGC 1275 may be the first galaxy for which a more complete model on resonant fluorescent excitation can be computed. Finding other galaxies with such a weak $H_2 2-1 S(3)$ line (e.g. in NGC 1068) would be important for constraining the process, which may provide an additional tool for understanding the radiative interaction between AGN and circumnuclear molecular material.

5. Br γ emission

The Br γ emission from NGC 1275 is unusual in that it is highly asymmetric both in its line profile (Fig. 1), and



Fig. 8. Upper level column density per mode of observed H_2 lines against upper level energy in K. A slope in this diagram is equivalent to an excitation temperature.

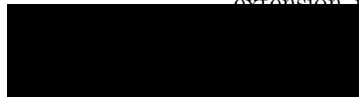
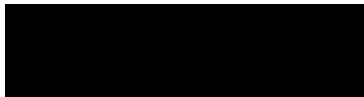


Fig. 9. Excitation diagrams showing the relative contributions of thermal and nonthermal excitation sources to H_2 emission (styled after Mouri 1994). The position of a source in these diagrams is *independent* of the intrinsic ortho/para ratio in the molecular clouds. In both diagrams the regions occupied by shocks (Brand et al. 1989), nonthermal (Black & van Dishoeck 1987), thermal UV (Sternberg & Dalgarno 1989), and X-ray (Lepp & McCray 1983, Draine & Woods 1990) excitation are outlined. Data of NGC 6240 and NGC 1068 are taken from Lester et al. (1988) and Oliva & Moorwood (1990). The location of NGC 1275 in these diagrams speaks for a largely thermal excitation of $\gtrsim 2000$ K.

in its spatial distribution (Fig. 10). The $\text{Br}\gamma$ emission is extended along roughly the same line ($\text{PA} = 160^\circ$) as the powerful radio jets (Pedlar et al. 1990), which suggests that the mechanism of its ionization is more strongly influenced by the central engine than by the surrounding stellar population. This result correlates well with $\text{H}\alpha$ and [NII] maps with visible band imaging spectroscopy (Ferruit & Pecontal 1994). In particular, the position of the extension in our maps correlates with an $\text{H}\alpha$ and [NII]

peak located $\approx 1''.2$ N, $0''.7$ W of the nucleus. From published $\text{H}\alpha$ maps, we estimate the $\text{H}\alpha$ flux in the hot spot to be $1.3 \times 10^{-17} \text{ W m}^{-2} \text{ arcsec}^{-2}$. Based on the observed [SII] line ratios and assuming a temperature of $\text{Te} = 10^4$ K, (Ferruit & Pecontal 1994) derive a mean electron density of $\text{n}_e = 40$ for this region, and a typical linewidth of 340 km s^{-1} .

The intrinsic $\text{Br}\gamma$ linewidth at the nucleus of $980 \pm 30 \text{ km s}^{-1}$ is unusually large for a pure star forming source. However, the width is not unexpected for emission from NLRs associated with AGNs and we therfore safely assume here that the NLR contributes a substastial fraction to the $\text{Br}\gamma$ emission. The larger linewidth of $\text{Br}\gamma$ compared to $\text{H}\alpha$ is probably a differential extinction effect. The emission was too faint to derive accurate $\text{Br}\gamma$ line profiles in regions $1''$ to the NW and SE of the nucleus in order to test whether the excess width and shape of the $\text{Br}\gamma$ line is due to expansion. The total $\text{Br}\gamma$ emission within the central 1 kpc is $9.7 \times 10^{-15} \text{ erg s}^{-1} \text{ cm}^{-2}$, which is a total luminosity of $1.5 \times 10^6 \text{ L}_\odot$. This corresponds to an ionization rate of $3.2 \times 10^{53} \text{ s}^{-1}$ or $2.0 \times 10^9 \text{ L}_\odot$ for $\text{Te} = 7500$ K, and can be compared with the value of $1.1 \times 10^{54} \text{ s}^{-1}$ inferred from M82 over a similar region from $\text{H}53\alpha$ recombination lines (Puxley 1991). From the ionization rate one can infer the total Lyman continuum luminosity L_{LyC} if one assumes



Fig. 10. Line map of $\text{Br}\gamma$ showing clear asymmetrical extension. Solid line marks the radio jet position angle of 160° . Contours are at 10, 20, 30...% of peak flux of $5.3 \times 10^{-15} \text{ erg s}^{-1} \text{ cm}^{-2} \text{ arcsec}^{-2}$.

OB type stars as its source. $L_{\text{LyC}} = 2.0 \times 10^9 L_\odot$ yields about 1.5% of the L_{FIR} of NGC 1275 ($1.5 \times 10^{11} L_\odot$) or $L_{\text{FIR}} / L_{\text{LyC}} \leq 75$. $L_{\text{LyC}} = 2 \times 10^9 L_\odot$ is a lower limit to the LyC-luminosity in the IRAS beam. The total bolometric luminosity of such an evolving stellar cluster is typically about 10 - 20 times higher than the Lyman continuum luminosity for typical assumptions on the properties of such a region if it were an active star forming region powered by massive stars (age \sim a few 10^7 y, $M_{\text{lower}} = 0.1 M_\odot$, $M_{\text{upper}} = 120 M_\odot$, see Fig. 10 in Krabbe et al. 1994). With that ratio $L_{\text{ionizing}} / L_{\text{Bol}} \sim 3.8 \times 10^{10} L_\odot$, which is about 25% of L_{FIR} . Taken as face values these numbers are not very consistent with star formation but much more with what one gets empirically, using above formulas for AGNs (Genzel et al. 1998).

6. The iron emission

6.1. Strength and morphology of the $[\text{Fe II}]$ emission

The $[\text{Fe II}]$ $1.644 \mu\text{m}$ emission from NGC 1275 is very strong (Fig. 2) and centrally concentrated (Fig. 11). Other prominent H and K band iron lines include the $[\text{Fe II}]$ $1.534 \mu\text{m}$, $[\text{Fe III}]$ $2.2178 \mu\text{m}$, and $[\text{Fe III}]$ $2.2420 \mu\text{m}$, in a near blend with H_2 2-1S(1). The flux of the $[\text{Fe II}]$ $1.644 \mu\text{m}$ (Table 2) is nearly as large as the $[\text{Fe II}]$ $1.257 \mu\text{m}$ in an $8''$ aperture by (Rudy et al. 1993). The $[\text{Fe II}]$ emission is much stronger compared to other star-

burst/Seyfert indicators than it is in most active galaxies. For example, in the central 1 kpc of NGC 1275, we find $[\text{Fe II}] (\lambda 1.644) / \text{Br}\gamma = 6.3$, whereas in roughly similar sized regions in the merger driven starburst NGC 3256 $[\text{Fe II}] / \text{Br}\gamma = 1.55$ and in the starburst/Seyfert systems NGC 4945 $[\text{Fe II}] / \text{Br}\gamma = 1.4$ (Moorwood & Oliva 1994) and NGC 1068 $[\text{Fe II}] / \text{Br}\gamma = 2.5$ (Thatte et al., in preparation; Blietz et al. 1994). While $\text{Br}\gamma$ originates predominantly from photoionization of H II regions by OB stars, $[\text{Fe II}]$ has an additional source. Most of the gas phase Fe in the local ISM condenses onto grains, so that the free Fe is often depleted by factors of 100 - 1000. If we presume that the ionization characteristics of the central source in NGC 1275 are similar to those of NGC 3256, NGC 4945, and NGC 1068, then the unusual $[\text{Fe II}] / \text{Br}\gamma$ and $[\text{Fe II}] / \text{Pa}\beta$ ratios (e.g. Rudy et al. 1993) would suggest that the iron depletion is $\lesssim 10$ in NGC 1275, less severe than in most starburst and active galaxies. This could be due to an ambient radiation field which heats the dust grains and tends to evaporate the Fe off of them. Such a scenario is supported by the relatively high derived dust temperature within the central 300 pc (e.g., Sect. 3.2). Alternatively, the fact that the ionization state of the gas must allow for plentiful Fe^+ , which can then be further ionized by photons with $E > 16.2 \text{ eV}$, requires that the ionizing source of radiation must be relatively cool, in order to produce low ionization radiation which would produce the high $[\text{Fe II}] / \text{Br}\gamma$ line ratios. However, fast J-shocks and X-ray heating can also produce copious $[\text{Fe II}]$ emission (Blietz et al. 1994). In the latter case, the X-rays penetrate deep into molecular clouds where they create large reservoirs of partially ionized gas.

6.1.1. Profile and excitation of the $[\text{Fe II}]$ emission

The profile of the $[\text{Fe II}]$ $1.644 \mu\text{m}$ line cannot be well modeled as a single Gaussian. This is typical of Seyfert galaxies, which often show narrow and broad components of the same emission feature. We therefore fit the observed profile using two Gaussians, a broad component of width $1340 \pm 120 \text{ km s}^{-1}$ and relative amplitude of 0.26, and a narrow component of width $280 \pm 20 \text{ km s}^{-1}$. This two component fit (Fig. 12), is excellent, and suggests that $\approx 50\%$ of the $[\text{Fe II}]$ emission arises in the same region as the $\text{Br}\gamma$, showing a similar linewidth, while the other half of the $[\text{Fe II}]$ arises in the same region as the H_2 , where the linewidths are again similar. Hence we propose — as in the case of the H_2 lines (Sect. 4.2) — that the active nucleus of NGC 1275 is responsible for much of the excitation leading to $[\text{Fe II}]$ emission. Comparing this result with Blietz et al. (1994), who have found an excellent correlation between the $[\text{Fe II}]$ emission and the NLR in NGC 1068 suggests, that we might have a similar case here but unresolved and at much greater distance.

The detailed line ratios expected from excitation via a central AGN have been modeled by Hollenbach & Maloney



Fig. 11. Line map of the FeII 1.644 μm line showing faint extensions beyond the immediate nuclear area. Contours are at 1.25, 5, 10, 20, 30...% of peak flux of 3.0×10^{-14} $\text{erg s}^{-1} \text{cm}^{-2} \text{arcsec}^{-2}$.

(1996). In their model, the X-ray energy absorbed per unit time per hydrogen nucleus in a cloud at distance $100r_{100}$ pc is $H_X \sim 7 \times 10^{-22} L_{44} r_{100}^{-2} N_{22}^{-1} \text{ erg s}^{-1}$, where $10^{44} L_{44} \text{ erg s}^{-1}$ is the AGN luminosity and $10^{22} N_{22} \text{ cm}^{-2}$ is the total column density. The heating rate is $\approx 0.3\text{--}0.4 H_X$, and the cooling is due to line emission from many species, but of particular diagnostic interest are the H_2 1-0S(1) and [Fe II] 1.64 μm lines. Using our value of $N_{\text{H}_2}^{\text{hot}} = 3 \times 10^{16} \text{ cm}^{-2}$, a molecular abundance of $\text{H}/\text{H}_2 \sim 10^5$, and $L_X \approx 2 \times 10^{43} \text{ erg s}^{-1}$ (Prieto 1996), and integrating the Hollenbach & Maloney results over our resolution beam of 300 pc, we can account for the observed [Fe II] to H_2 1-0S(1) line ratio. For all radii larger than our beam, the predicted ratio is $\approx 1:1$. This is close to our measured value of 1.5:1 in a 3'' aperture (Table 2) since the predicted ratio depends on the presumed depletion of Fe, which we already know to be $\lesssim 10$, and which the model presumes to be ≈ 30 (Hollenbach, private communication). We thus conclude that the [Fe II] emission as well as [Fe II]/ H_2 1-0S(1) can be explained by an X-radiation field typically emitted by AGN.

7. The CO_{sp} index

The CO_{sp} index of the underlying stellar population can be diluted by continuum emission not originating in stars. If the non-stellar continuum is χ times stronger than the



Fig. 12. Profile of the FeII 1.644 μm line showing multicomponent fit. The solid dark line is the data, to which the best single component fit has a full width of 544 km s^{-1} . The two lower intensity profiles are the broad and narrow component required to fit the profile well. The dotted line which closely follows the data is the sum of the broad ($1345 \pm 120 \text{ km s}^{-1}$) and narrow ($280 \pm 20 \text{ km s}^{-1}$) components.

stellar continuum, the CO_{sp} index will be diminished according to

$$CO_{sp}(\chi) = -2.5 \log \frac{S_0 + \chi}{1 + \chi} \quad (2)$$

where $S_0 = 10^{-0.4 CO_{sp}(0)}$ is the average of the undiluted rectified spectrum between 2.31 and 2.40 μm and CO_{sp} is the spectroscopic index. Details are given in Doyon et al. (1994). According to our model fitting, the non-stellar continuum in the central 1'' contributes $\gtrsim 90\%$ of the emission, reducing the observed CO_{sp} from its intrinsic value of ≈ 0.3 to ≈ 0.03 , and giving rise to the CO_{sp} hole at the nucleus of NGC 1275 (Fig. 13). The range for the allowed values of the intrinsic CO_{sp} is indicated in Fig. 14. The nuclear stellar cluster may have a higher CO index than initially assumed, implying that the K supergiants with CO_{sp} ≈ 0.3 instead of giants may be the dominating population (Doyon et al. 1994). Including this finding into a reiteration on the continuum decomposition will not have any effect on the results, since the temperature of these stellar types are not very different.

Outside of the hole, the CO_{sp} of 0.17 is typical of E/S0 galaxies (Frogel et al. 1978), confirming that the stellar population of NGC 1275 is quite normal. Furthermore CO_{sp} = 0.17 corresponds to a K5 III star (Doyon et al. 1994, appendix A), which corroborates our spectral synthesis results for regions at $R \gtrsim 3''$.

Given that the light is dominated by K giants or supergiants, we try to estimate the total nuclear stellar mass. Using our result that the emission enclosed in the central $3''$ (1 kpc) of NGC 1275 is $\gtrsim 90\%$ due to non-stellar sources, we correct the observed K magnitude of the *stellar component only* of $m_K = 11.8$ [in agreement with other recent values $m_K = 11.9$ (Forbes et al. 1992)] to $m_K = 14.3$. Converting to absolute visual magnitudes yields $M_V^{K5\text{ III}}(\text{NGC 1275}) = (V-K) + m_K - 25 - A_K - 5$ $\log D_{\text{Mpc}} = -16.8$ using $V-K = 3.24$, $A_K \sim 0.2$, and $D = 68.8$ Mpc. The mass of a K giant is $1.2 M_{\odot}$, and its $M_V^{K5\text{ III}} = -0.2$ (Lang 1992), which implies $4.6 \times 10^6 M_{\odot}$ of K5 III stars in the central $3''$.

Assuming a Salpeter IMF with $P(M) \propto M^{-1.35}$ dM , the mass fraction of the stars in the range 1.0 to $1.5 M_{\odot}$ (roughly the range of stellar masses which will become K5 III stars), for a population bounded by $0.1 M_{\odot}$ and $100 M_{\odot}$ stars is $(1.0^{-0.35} - 1.5^{-0.35})/(0.1^{-0.35} - 100^{-0.35}) = 0.065$, so that K5 III stars make up about 7% of the mass of a star cluster. Hence the total mass of stars in the central kpc is thus $7.1 \times 10^7 M_{\odot}$. If the population is dominated by K supergiants, the total stellar mass comes out to be the same value (mass range = $12 - 14 M_{\odot}$ $M_V^{K5\text{ I}} = -5.0$).

We estimate the core radius r_0 of the nuclear stellar cluster to be smaller than 500 pc. Using this value as an upper limit and knowing the stellar mass of the cluster, we can use $\rho_0 = 9\sigma_0^2/4\pi G r_0^3$ (Eckart et al. 1993) to estimate the expected velocity dispersion: $\sigma = \sqrt{M_{\text{cluster}} G / 9r_0} \gtrsim 8.4$ km/s. Even if the CO absorption had been detected on the nucleus, such a small dispersion had been beyond the capabilities of our instrument.

We conclude that the absence of CO bandheads in the nuclear emission indicates that those bandheads are heavily diluted by the emission of hot dust and power-law emission.

8. Discussion

Our spectral synthesis (Sect. 3) shows that inside of the central 300 pc , the NIR continuum emission is dominated by the AGN and hot dust components. Together these are $\gtrsim 10$ times more powerful than the stellar emission from the same region. This result is confirmed by the observed factor of $\gtrsim 10$ continuum CO_{Sp} dilution (Sect. 7) at the nucleus. The nature of the nuclear power source likely is a massive black hole (MBH) with a surrounding molecular gas cloud torus or disk. The lack of strong CO absorption bands indicates that massive star formation probably does not play a very important role in the nucleus.

The intensity and morphology of the line emission suggest that more than one mechanism is at work exciting the line emission. In addition to the AGN, shocks are also likely to play a large role. Since the J band [Fe II] lines are unusually strong, even for an AGN, it requires a substan-



Fig. 13. The azimuthally averaged CO_{Sp} index in NGC 1275. The apparent decrease in CO_{Sp} toward the center is an artifact of continuum dilution due to hot dust and the scattered light of the AGN.

tial boost of the H₂ emission to keep the [Fe II]/H₂ 1–0 S(1) ratio near unity. This is indeed observed in NGC 1275, which has unusually strong H₂ emission compared to other Seyferts. Furthermore, the spatial extension of the H₂ emission (Sect. 4.1) suggests that it may be driven by shocks from a recent or ongoing merger event. Such a picture is supported by not only the observed isophotal shell structure (Hernquist & Weil 1992), but also by the extinction analysis of Norgaard-Nielsen et al. (1993), which shows that the HV system is at least partially *moving through* the main galaxy rather than completely in front of it. Hence the interaction of the HV and LV systems could give rise to the required shocks which boost the H₂ emission. This process is postulated to occur in the merging galaxy NGC 6240 (van der Werf et al. 1993). Among AGNs, strong [Fe II] emission is not unique to NGC 1275. In fact there are a large number of AGNs with elevated [Fe II] emission (among them many IRAS luminous and starburst galaxies such as MRK 231, MRK 507, and PHL 1092), which can be attributed to violent star formation in a metal rich environment (Fillipenko & Terlevich 1992, Lipari et al. 1993). In the merger induced H₂ boosting scenario, the unusually high level of [Fe II] emission observed from NGC 1275 would likely be due to a different effect, namely the dissociation of Fe from interstellar grains via shock heating. This could produce an iron rich gas phase (Sect. 6.1.1), which would then give rise to the very strong observed [Fe II] emission.



Fig. 14. The black lines in the graph represent solutions of equation (2). The inner area of the triangle illustrate the range of allowed values of the measured CO spectroscopic index $\text{CO}_{\text{sp}}(\chi)$ in NGC 1275. Constrains are the limits set by the error of the index itself, the range of likely values for the spectroscopic index $\text{CO}_{\text{sp}}(0)$ in a nondiluted stellar cluster, and the error in χ (see Fig. 13 and Sect. 3.2.)

The fact that the $\text{Br}\gamma$ emission is generally extended suggests the presence of young stars and thus extended recent star formation. If the slight extension of the continuum is significant, it suggests increased star formation along the jets, perhaps due to shocks, caused by interactions with the surrounding medium. Part of the $\text{Br}\gamma$ emission along the radio jet may be influenced by the radiation from the nucleus and thus not created by star formation. The extended component of hot molecular hydrogen is probably shock excited as a result of the star formation.

The existence (or non-existence) of “cooling flows” — an inflow of cool gas into a galaxy from its halo of hot x-ray emitting gas — is currently a topic of intense debate. The evidence *for* them is that some galaxies which are surrounded by a halo of hot, X-ray emitting gas show a dramatic central drop in the gas temperature. As the primary cooling mechanism of this gas is bremsstrahlung ($\text{emission} \propto n^2$), and as the central temperature drop is accompanied by a brightness increase, the gas must be both cooler and denser (see, e.g. Sarazin et al. 1992 for a physical introduction and review). If the gas is cooler and denser, then it must fall toward the center of the galaxy. In the case of NGC 1275, the predicted infall amounts to $\approx 200 \text{ M}_\odot \text{ yr}^{-1}$ (Fabian et al. 1981), or $2 \times 10^{12} \text{ M}_\odot$ in 10^{10} years. The evidence *against* cooling flows is that if such enormous quantities of gas really are falling in, they must be detectable in some way, yet careful searches have not revealed the gas in any of its expected states. We know that the gas cannot form stars with a normal IMF,

because 200 M_\odot of star formation would be 20 times more powerful than the prototypical starburst galaxy, M 82, and easily detected via color variations (Cardiel et al. 1995).

Our H_2 data provide several evidences against the cooling flow hypothesis.

i) The spatial distribution of the hot molecular hydrogen strongly peaks at the nucleus of NGC 1275 on a scale $<300\text{pc}$. If the H_2 emission was due to the cooling flow, one would have expected a much more extended distribution since the gas has to fall through all of the galaxy. The weakness of the H_2 2–1 S(3) line (see Sect. 4.3) emphasises the close relation of the hot H_2 with the nucleus.

ii) The temperature variation within the hot H_2 is small. Between 0 K and about 20000 K upper level energy the temperature only varies by about 1500 K. A cooling hot gas cloud is likely to show a much larger span of temperature compared to what our data show.

iii) The temperature of the hot H_2 is rather low: between 1500 K and 3000 K. There is no evidence of a very hot ($\gtrsim 3000$ K) H_2 component which can be expected for a cooling hot gas mass.

iv) The line emission of the hot H_2 can be explained consistently with mostly thermal excitation (e.g. in a post-shock environment) with a smaller component of X-ray heating. A “cooling flow” scenario does not need to be invoked to explain the line emission of molecular hydrogen in NGC 1275.

Several groups have argued that the gas cannot have collected in the form of molecular hydrogen (H_2), because searches for CO emission associated with H_2 have revealed only very limited quantities of H_2 gas, although NGC 1275 is unusual in that it shows more CO than most cooling flow galaxies (Lazareff et al. 1989, Inoue et al. 1996, O’Dea et al. 1994). However, since the temperature regime is very different from the cold molecular clouds, the $\text{CO} \rightarrow \text{H}_2$ conversion factor is certainly different and may even not be applicable in this context.

The gas could have been collected as atomic hydrogen. However, only very limited quantities have been detected, certainly much less than would be expected from an infall of several hundred solar masses per year over cosmic timescales (Haschick et al. 1982).

One of the last places in which the purported inflow could be hiding is in stars with a very unusual kind of IMF, one that is biased toward producing low mass stars, so that the star formation rate as determined by the total number of ionizing photons (these are produced only by massive stars) does not reflect the total amount of mass involved in the star formation process. A population of such low mass stars should have a somewhat lower CO_{sp} index than a normal population, because it will have fewer luminous giants and supergiants which are the largest contributors to the CO absorption lines. Our NIR spectroscopy allows us to analyze the stellar population of regions 1 kpc from the nucleus via the CO_{sp} index, where we find a $\text{CO}_{\text{sp}} = 0.17$. This can be compared with theoretical pre-

dictions for a population of very low mass stars (see Fig. 20 in Kroupa & Gilmore 1994), whose expected value of CO_{sp} is between 0.07 and 0.16 for cooling flow rates of 158 M_⊙ yr⁻¹. For higher mass deposition rates, the expected CO_{sp} decreases, so that for a rate of 316 M_⊙ yr⁻¹ the expected CO_{sp} lies between 0.0 and 0.1. Hence we cannot completely eliminate the existence of a low mass star population for a cooling flow of 200 M_⊙ yr⁻¹ as is postulated for NGC 1275, but the observed CO_{sp} index is at the extreme limit of theoretically acceptable values.

9. Summary

We observed the central 1 kpc of NGC 1275 with the MPE 3D imaging spectrograph. We find that the central ≈ 300 pc are strongly dominated by emission from an AGN and from hot dust: There is no evidence of a nuclear stellar continuum. In the regions at a distance of ≈ 1 kpc from the nucleus, the situation is completely reversed, and the emission is totally dominated by a stellar population whose spectra is consistent with a normal, old ($> 10^8 - 10^9$ y) population. In this region, we find no evidence to support the thesis that substantial quantities of infalling “cooling flow” gas has been transformed into stars with an IMF biased toward low masses, although we cannot strictly rule out a low mass population because the purported flow may be disturbed in the central 10 kpc of the galaxy. Within the central ~ 500 pc, the emission line ratios of many important diagnostic lines from the NIR regime are consistent with excitation from a combination of AGN emission and shock excitation. The shocks may be due to previous mergers, or to the early phases of a merger between the HV and LV systems.

Acknowledgements. We thank the 3D team for their enthusiastic support during the observations.

Appendix A: Spectral Fitting of the continuum emission

The total intrinsic continuum emission at each wavelength λ is

$$I_{\lambda}^{\text{INT}} = \sum_i c_i I_{\lambda}^i \quad \text{with} \quad \sum_i c_i = 1. \quad (\text{A1})$$

In active and starburst galaxies, we identify four sources of continuum emission: stellar ($I_{\lambda}^{\text{STAR}}$), AGN power-law (I_{λ}^{P}) and hot dust (I_{λ}^{HD}), and free-free (I_{λ}^{FF}). The intrinsic emission of

$$I_{\lambda}^{\text{INT}} = c_{\text{S}} I_{\lambda}^{\text{STAR}} + c_{\text{PL}} I_{\lambda}^{\text{P}} + c_{\text{HD}} I_{\lambda}^{\text{HD}} + c_{\text{FF}} I_{\lambda}^{\text{FF}} \quad (\text{A2})$$

is then extinguished according to

$$I_{\lambda}^{\text{SYN}} = \begin{cases} I_{\lambda}^{\text{INT}} e^{-g\tau_{\lambda}} e^{-\tau_{\lambda}}, & \text{Screen} \\ I_{\lambda}^{\text{INT}} e^{-g\tau_{\lambda}} (1 - e^{-\tau_{\lambda}})/\tau_{\lambda}, & \text{Mix.} \end{cases} \quad (\text{A3})$$

to obtain the synthetic spectrum. The extinction has two parts, one due to dust within our Galaxy ($g\tau_{\lambda}$), and one due to dust within the source galaxy (τ_{λ}). In our model, the latter can have either a simple screen geometry or a mixed stars/gas geometry. In all cases, the extinction is taken to vary as $\lambda^{-1.85}$ (Landini et al. 1984), and is fixed to be $A_{\text{K}} = 0.112 A_{\text{V}}$ at $\lambda = 2.2 \mu\text{m}$ (Rieke & Lebofsky 1985).

When comparing I_{λ}^{SYN} with the observed spectrum, I_{λ}^{OBS} , we avoid emission lines due to non-continuum sources (e.g. shocked ISM gas, photoionized gas clouds), and define our goodness of fit parameter, χ^2 , such that

$$\chi^2 = \frac{1}{N-1} \sum_{\lambda \neq \text{line}} \frac{(I_{\lambda}^{\text{SYN}} - I_{\lambda}^{\text{OBS}})^2}{\sigma_{\lambda}^2} \quad (\text{A4})$$

where N is the number of measured spectral points which contain no line emission or absorption from non-continuum sources and σ_{λ} is the local noise.

To model the stellar component, we have resampled the $R \approx 3000$ normalized K band spectra of Kleinmann & Hall (1986) at the 3D resolution of $R = 670$ onto our $0.001 \mu\text{m} \text{ pix}^{-1}$ data format (Förster et al. 1996), and then multiplied them by a Rayleigh-Jeans power law of $\lambda^{-3.94}$ (Doyon et al. 1994) corresponding to an A0V star to reconstruct the true stellar spectrum.

The intrinsic spectrum of the hot dust of temperature T_{d} , is taken to be a black body multiplied by a power-law emissivity of the form $\epsilon_{\text{dust}} \propto \lambda^{-1}$. Hence, $I_{\lambda}^{\text{HD}} = B_{\lambda}(T_{\text{d}})\lambda^{-1}$, where $B_{\lambda}(T_{\text{d}})$ is the black body function.

The behavior of free-free emission is given by $I_{\nu} \propto e^{-h\nu/kT}$ where T is the plasma temperature (normally > 5000 K). We convert to wavelength units, and find $I_{\lambda} \propto \lambda^{-2} e^{-hc/\lambda kT}$ which we adopt as our functional form for free-free emission.

References

Acosta-Pulido J. A., Perez-Fournon I., Calvani M., Wilson A. S., 1990, *ApJ* 365, 119

Beckwith S., Persson S. E., Neugebauer G., Becklin E. E., 1978, *ApJ* 223, 464

Black J. H., van Dishoeck E. F., 1987, *ApJ* 322, 412

Blietz M., Cameron M., Drapatz S., et al., 1994, *ApJ* 421, 92

Böhringer H., Voges W., Fabian A. C., Edge A. C., Neumann D. M., 1993, *MNRAS* 264, 25

Böker T., Krabbe A., Storey J., 1998, *ApJ* 498, L115

Braine J., Wyrowski F., Radford S. J. E., Henkel C., Lesch H., 1995, *A&A* 293, 315

Brand P. W. J. L., Toner M. P., Geballe T. R., et al., 1989, *MNRAS* 236, 929

Burton M., Hollenbach D., Tielens A., 1992, *ApJ* 399, 563

Cardiel N., Gorgas J., Aragon-Salamanca A., 1995, *MNRAS* 296, 628

Chrysostomou A., Brand P., Burton M., Moorhouse A., 1993, *MNRAS* 265, 329

Crawford C. S., Fabian A. C., 1993, *MNRAS* 265, 431

Doyon R., Joseph R. D., Wright G. S., 1994, *ApJ* 421, 101

Draine B. T., Bertoldi F., 1996, *ApJ* 468, 269

Draine B. T., Woods D. T., 1990, *ApJ* 363, 464

Draine B. T., Woods D. T., 1991, *ApJ* 383, 621

Eckart A., Genzel R., Hofmann R., Sams B., Tacconi-Garman L., 1993, *ApJ* 407, L77

Fabian A. C., Hu E. M., Cowie L. L., Grindlay J., 1981, *ApJ* 248, 47

Ferruit P., Pecontal E., 1994, *A&A* 288, 65

Filippenko A. V., Terlevich R., 1992, *ApJ* 397, L79

Fischer J., Smith H. A., Geballe T. R., Simon M., Storey J. W. V., 1987, *ApJ* 320, 667

Flower D., Watts G., 1984, *MNRAS* 209, 25

Forbes D. A., Ward M. J., Depoy D. L., Boisson C., Smith M. S., 1992, *MNRAS* 254, 509

Förster N. M., Böker T., Krabbe A., Genzel, 1996, in C. Leitherer, U. F. von Alvensleben, J. Huchra (eds.), *From Stars to Galaxies*, Vol. 98 of *ASP Conference Series*, p. 417

Frogel J. A., Persson S. E., Matthews K., Aaronson M., 1978, *ApJ* 220, 75

Genzel R., Lutz D., Sturm E., et al., 1998, *ApJ* 498, 579

Granato G., Danese L., Franceschini A., 1997, *ApJ* 486, 147

Gredel, R., et al., 1994, *A&A* 292, 580

Haschick A. D., Crane P. C., van der Hulst J. M., 1982, *ApJ* 262, 81

Hernquist L., Weil M. L., 1992, *Nat* 358, 734

Hollenbach D. J., Maloney P. R., 1996, in R. Chiao (ed.), *Amazing Light*, Springer, New York

Hora J., Latter W., 1996, *ApJ* 461, 288

Inoue M. Y., Kameno S., Kawabe R., et al., 1996, *AJ* 111, 1852

Joy M., Harvey P., 1987, *ApJ* 315, 480

Joy M., Lester D. F., 1988, *ApJ* 331, 145

Kawara K., Taniguchi Y., 1993, *ApJ* 410, L19

Kleinmann S. G., Hall D. N. B., 1986, *ApJS* 62, 501

Krabbe A., Sternberg A., Genzel R., 1994, *ApJ* 425, 72

Krabbe A., Weitzel L., Kroker H., et al., 1995, in A. Fowler (ed.), *Proc. of SPIE conference on Infrared Imaging Systems*, Vol. 2475, p. 172

Kroupa P., Gilmore G., 1994, *MNRAS* 269, 655

Landini M., Natta A., Salinari P., Oliva E., Moorwood A. F. M., 1984, *A&A* 134, 284

Lang K. R., 1992, *Astrophysical Data: Part 1: Planets and Stars*, Springer, New York

Laor A., Draine B. T., 1993, *ApJ* 402, 441

Lazareff B., Castets A., Kim D. W., Jura M., 1989, *ApJ* 336, L13

Lepp S., McCray R., 1983, *ApJ* 269, 560

Lester D. F., Harvey P. M., Carr J., 1988, *ApJ* 329, 641

Levinson A., Laor A., Vermeulen R. C., 1995, *ApJ* 448, 589

Lipari S., Terlevich R., Macchetto F., 1993, *ApJ* 406, 451

Longmore A. J., Sharples R. M., Tokunaga A. T., et al., 1984, *MNRAS* 209, 373

Maiolino R., Ruiz M., Rieke G., Keller L., 1995, *ApJ* 446, 561

Maoz D., Filippenko A. V., Ho L. C., et al., 1995, *ApJ* 440, 91

Martini P., Sellgren S., Hora J., 1997, *ApJ* 484, 296

McCaughrean M. J., Glindemann A., Birk C., et al., 1994, *Experimental Astronomy* 3, 137

McLeod K., Rieke G., Rieke M., Kelly D. M., 1993, *ApJ* 412, 111

Minkowski R., 1957, in H. C. van der Hulst (ed.), *IAU Symposium*, Vol. 4 of Cambridge University Press, p. 107

Moorwood A. F. M., Oliva E., 1990, *A&A* 239, 78

Moorwood A. F. M., Oliva E., 1994, *ApJ* 429, 602

Mouri H., 1994, *ApJ* 427, 777

Norgaard-Nielsen H. U., Hansen L., Jorgensen H. E., 1990, *A&A* 240, 70

Norgaard-Nielsen H. U., Goudfrooij P., Jorgensen H. E., Hansen L., 1993, *A&A* 279, 61

O'Dea C. P., Baum S. A., Maloney P. R., Tacconi L. J., Sparks W. B., 1994, *ApJ* 422, 467

Oliva E., Moorwood A. F. M., 1990, *ApJ* 338, L5

Oliva E., Origlia L., Kotilainen J. K., Moorwood A. F. M., 1995, *A&A* 301, 55

Pedlar A., Ghataure H. S., Davies R. D., et al., 1990, *MNRAS* 246, 477

Pier E. A., Krolik J. H., 1992, *ApJ* 401, 99

Prieto A. M., 1996, *MNRAS* 282, 421

Puxley P. J., 1991, *MNRAS* 249, p11

Puxley P. J., Hawarden T. G., Mountain C. M., 1990, *ApJ* 364, 77

Reuter H. P., Pohl M., Lesch H., Sievers A. W., 1993, *A&A* 277, 21

Rieke G. H., Lebofsky M. J., 1985, *ApJ* 288, 618

Romanishin W., 1986, *ApJ* 301, 675

Rudy R. J., Cohen R. D., Rossano G. S., et al., 1993, *ApJ* 414, 527

Sarazin C. L., Wise M. W., 1993, *ApJ* 411, 55

Sarazin C. L., O'Connell R. W., McNamara B. R., 1992, *ApJ* 389, L59

Seyfert C. K., 1943, *ApJ* 97, 28

Sternberg A., Dalgarno A., 1989, *ApJ* 338, 197

Sternberg A., Dalgarno A., Lepp S., 1987, *ApJ* 320, 676

Sugai H., Malkan M., Ward M., Davies R., McLean I., 1997, *ApJ* 481, 186

Taylor G. B., Vermeulen R. C., 1996, *ApJ* 457, L69

Thatte N., Quirrenbach A., Genzel R., Maiolino R., Tecza M., 1997, *ApJ* 490, 238

Timmermann R., Bertoldi F., Wright C., et al., 1996, *A&A* 315, L281

Turner J., Kirby-Docken K., Dalgarno A., 1977, *ApJS* 35, 281

van der Werf P. P., Genzel R., Krabbe A., et al., 1993, *ApJ*
405, 522

Venturi T., Readhead A. C. S., Marr J. M., Backer D. C., 1993,
ApJ 411, 552

Vermeulen R. C., Readhead A. C. S., Backer D. C., 1994, *ApJ*
430, L41

Veron P., 1978, *Nat* 272, 430

Weitzel L., Krabbe A., Kroker H., et al., 1996, *A&AS* 119, 531

Wright C., Drapatz S., Timmermann R., et al., 1996, *A&A*
315, L301

Wynn-Williams C., Becklin E. E., 1986, *ApJ* 308, 620

This figure "h1635_01.GIF" is available in "GIF" format from:

<http://arxiv.org/ps/astro-ph/0001052v1>

This figure "h1635_02.GIF" is available in "GIF" format from:

<http://arxiv.org/ps/astro-ph/0001052v1>

This figure "h1635_03.GIF" is available in "GIF" format from:

<http://arxiv.org/ps/astro-ph/0001052v1>

This figure "h1635_04.GIF" is available in "GIF" format from:

<http://arxiv.org/ps/astro-ph/0001052v1>

This figure "h1635_05.GIF" is available in "GIF" format from:

<http://arxiv.org/ps/astro-ph/0001052v1>

This figure "h1635_06.GIF" is available in "GIF" format from:

<http://arxiv.org/ps/astro-ph/0001052v1>

This figure "h1635_07.GIF" is available in "GIF" format from:

<http://arxiv.org/ps/astro-ph/0001052v1>

This figure "h1635_08.GIF" is available in "GIF" format from:

<http://arxiv.org/ps/astro-ph/0001052v1>

This figure "h1635_9a.GIF" is available in "GIF" format from:

<http://arxiv.org/ps/astro-ph/0001052v1>

This figure "h1635_9b.GIF" is available in "GIF" format from:

<http://arxiv.org/ps/astro-ph/0001052v1>

This figure "h1635_10.GIF" is available in "GIF" format from:

<http://arxiv.org/ps/astro-ph/0001052v1>

This figure "h1635_11.GIF" is available in "GIF" format from:

<http://arxiv.org/ps/astro-ph/0001052v1>

This figure "h1635_12.GIF" is available in "GIF" format from:

<http://arxiv.org/ps/astro-ph/0001052v1>

This figure "h1635_13.GIF" is available in "GIF" format from:

<http://arxiv.org/ps/astro-ph/0001052v1>

This figure "h1635_14.GIF" is available in "GIF" format from:

<http://arxiv.org/ps/astro-ph/0001052v1>